

Article

Correlations of the Electronic, Elastic and Thermo-Electric Properties of Alpha Copper Sulphide and Selenide

Moshibudi Ramoshaba and Thuto Mosuang * 

Department of Physics, University of Limpopo, University Road, Mankweng, Polokwane 0727, South Africa

* Correspondence: thuto.mosuang@ul.ac.za; Tel.: +27-(0)15-268-3576

Abstract: A full potential all-electron density functional method within generalized gradient approximation is used herein to investigate correlations of the electronic, elastic and thermo-electric transport properties of cubic copper sulphide and copper selenide. The electronic band structure and density of states suggest a metallic behaviour with a zero-energy band gap for both materials. Elastic property calculations suggest stiff materials, with bulk to shear modulus ratios of 0.35 and 0.44 for Cu₂S and Cu₂Se, respectively. Thermo-electric transport properties were estimated using the Boltzmann transport approach. The Seebeck coefficient, electrical conductivity, thermal conductivity and power factor all suggest a potential p-type conductivity for α -Cu₂S and n-type conductivity for α -Cu₂Se.

Keywords: CuS; CuSe; density functional theory; electronic structure; elastic constants; transport properties; power factor

1. Introduction

Copper-based chalcogenides, especially copper sulphides (CuS) and selenides (CuSe), have the potential to replace some of the leading silicon families of energy-harvesting materials, which are becoming extinct at present. These binary compounds are generated from group IB transitional metals and group VIA non-metals. The three elements, copper, sulphur and selenium, are readily available from the Earth's crust. Uniquely designed CuS and CuSe chalcogenides allow the development of cost-effective energy compounds with minor environmental hazards [1]. Studies show that both CuS and CuSe can exist in a variety of stoichiometries, with crystal forms ranging from the cubic to the hexagonal phase [1–7]. Heating and cooling processes within the materials mostly lead to a transition from one form to the other [2,3].

A CuSe configuration is a blended conductor that displays diverse phase transitions from stable to metastable forms and from low- to high-temperature forms. In particular, Cu₂Se undergoes a low-temperature monoclinic to high-temperature face-centred cubic (fcc) phase transition at 410 K [3]. On the other hand, Cu₂S undergoes two phase transitions: one at around 370 K and another at 700 K [4,5]. At 370 K, a transition from the monoclinic to hexagonal phase takes place, coupled with the hexagonal to cubic phase at 700 K. The intermediate phases, which include monoclinic and orthorhombic, can also be categorized as superionic due to them having fast mobile fluidic Cu¹⁺ or Cu²⁺ ions within the focal Se²⁻ ions lattice.

Namsani et al. [2] and Kim et al. [6] revealed that at room temperature CuSe is not well defined, but at high temperatures, the cubic phase is dominant. The prevailing lattice originates from Se ions, with Cu ions arbitrarily dispersed at different sites within this lattice matrix. Upon the cubic-faced Se ion lattice, Cu ions exhibit fluidic behaviour, which results in the good thermo-electric character of the compound. Such a performance shows cubic CuSe as a favourable material when it comes to thermal and electronic parameter regulation. Even though the Se atom lattice is well defined, the cubic CuSe still demonstrates



Citation: Ramoshaba, M.; Mosuang, T. Correlations of the Electronic, Elastic and Thermo-Electric Properties of Alpha Copper Sulphide and Selenide. *Computation* **2023**, *11*, 233. <https://doi.org/10.3390/computation11110233>

Academic Editors: Cuiying Jian and Aleksander Czekanski

Received: 1 September 2023

Revised: 5 October 2023

Accepted: 20 October 2023

Published: 17 November 2023



Copyright: © 2023 by the authors. Licensee MDPI, Basel, Switzerland. This article is an open access article distributed under the terms and conditions of the Creative Commons Attribution (CC BY) license (<https://creativecommons.org/licenses/by/4.0/>).

inconsistencies with respect to thermo-physical and structural properties with increasing temperatures. Such inconsistencies result in a large coefficient of thermal expansion at high temperatures and a decrease in heat capacity towards the theoretical limit of liquids. Despite such reported anomalies, notable developments in measurements and computations are continuously achieved to further understand the material's properties. The computational studies of Tyagi et al. [7] achieved high-temperature cubic Cu₂Se using PBE and its hybrid functional. This study highlighted a semi-metallic, n-type conductivity, which creates a ~0.5 eV band gap whenever the hybrid PBE functional is exercised. In contrast, copper impurities in CdSe were investigated by Nelson et al. [8] using the TDDFT approach. In this case, the excited state configurations were used to understand the photo-physical behaviour, like luminescence and conductivity, observed in measurements.

Regarding the CuS chalcocite, experiments further showed Cu atoms being highly mobile within the temperature range of 300–373 K because of its chemical stoichiometry [9]. Due to their elevated Cu atoms' mobility, locating their positions is difficult; thus, their statistical distributions are studied. This explains the existence of the diverse crystal phases observed within this compound. A mixture of cubic and hexagonal chalcocite is present above 363 K, but as the temperature increases, the hexagonal phase continues to disappear until only cubic CuS chalcocite is observable above 410 K. Similarly, the orthorhombic CuS transforms into cubic chalcocite at temperatures above 346 K. On the other hand, Will et al. [4] recorded that below 346 K the monoclinic chalcocite spontaneously transforms and exhibits cubic symmetry. The first-principle calculations by Arora et al. [10] depicted covellite CuS as exhibiting complex hexagonal symmetry with respect to the metallic superconducting character at various temperatures. The same findings were achieved by Lv et al. [11] with anisotropic yet stable elasticity, which corresponds to the measured data. Metallic behaviour is associated with the hybridization of the copper 3d and sulphur 3p eigenstates.

Coincidentally, in both CuS and CuSe chalcogenides, the cubic symmetry phase is considered the most stable, which is always evident at ambient and high temperatures, and they are favoured for thermo-electric transport applications [2,3,9]. Due to the potential of these exciting CuS and CuSe chalcogenides in a wide range of applications, such as thermo-electric solar cells, conductive fibres, optical filters and high-capacity cathode materials in lithium secondary batteries, further inquiry is deemed necessary [9,12]. In this article, the electronic structure, and elastic and thermo-electric transport properties of the cubic Cu₂S and Cu₂Se phases are explored. To conduct such investigations, ab initio density functional theory (DFT) methods, which apply the all-electron, full potential, linearized augmented-plane wave approach, are used. The study may serve as an insight into how the electronic structure and elastic properties can be manipulated in effective thermo-electric-energy-based transport compounds.

2. Computational Details

The computational details of the electronic, elastic and transport properties of cubic copper sulphide (α -Cu₂S) and selenide (α -Cu₂Se) phases are presented in this section. The calculations performed were based on the open source Exciting package [13]. Density functional theory (DFT) using generalized gradient approximation (GGA) as the exchange–correlation functional energy was utilized [14,15]. The Perdew–Burke–Ernzerhof form applied in solid materials (PBE_sol) [15] was the chosen GGA. The full potential, all-electron, linearized augmented-plane waves on both cubic Cu₂S and Cu₂Se were applied. For electronic structure and elastic property calculations, a good choice of the ground-state parameters will assist when comparing the results and associated physical quantities. The total energy convergence was also based on the convincing sampling mesh of the k-points and the expansion of the eigenfunctions using the chosen size of the basis set. In this way, the calculation time scales linearly with respect to the k-points' weighing and exponentially with respect to the basis set.

In both compounds, the interstitial bonding between the Cu and S or Se atoms is described by plane waves. The Cu, S and Se atomic sites' central potentials use the muffin-tin basis function description [13]. To a good approximation, the working muffin-tin basis contains a sum of radial eigenfunctions and the derivative of the radial eigenfunctions with respect to energy, which all operate on the spherical harmonic component of the wavefunctions. This choice produces a smooth and continuous muffin-tin basis function for the interstitial plane waves. The analysis of electronic thermo-electric properties is carried out using the Boltzmann theory [16]. This is because the calculations are based on the semi-classical approach to the solution of the linearized Boltzmann transport equation. The equations contain the derivative of the Fermi distribution function. The rigid body and relaxation time approximations are considered. A relaxation time of $\tau = 10$ fs is imposed for the calculations of the Seebeck coefficient (S), the power factor per relaxation time ($\sigma S^2/\tau$), electrical conductivity per relaxation time (σ/τ) and thermal conductivity per relaxation time (κ/τ).

Cubic α -Cu₂S and α -Cu₂Se compounds possess space group Fm-3m (No. 225) with a fluorite prototype structure. Ideally, Cu¹⁺ is bonded equivalently to S²⁻ or Se²⁻ ions to create a cell edge and corner-sharing mixture in a CuSe₄ tetrahedron. Conversely, the S²⁻ or Se²⁻ ion is bonded equally in a body-centered cubic form to eight Cu¹⁺ ions. The regular structure contains two highly symmetric positions, where S²⁻ (Se²⁻) and Cu¹⁺ ions occupy localized positions 4a (0.00 0.00 0.00) and 8c (0.25 0.25 0.25), respectively, according to the Wyckoff table of coordinates [17]. The optimized lattice constants for α -Cu₂S and α -Cu₂Se used in the calculations are $a = b = c = 10.497$ Bohr and $a = b = c = 10.850$ Bohr, respectively. Here, 1 Bohr = 1 atomic unit (a.u.) = 0.529 Å.

3. Results and Discussion

All electronic, elastic and transport properties of alpha Cu₂S and Cu₂Se were examined at room temperature. The electronic properties describe the state and behaviour of electrons in the material. For example, the electronic band structure and the density of state describe the state of the electrons in terms of their energies. Elastic properties determine the mechanical properties of the material. The transport properties assist with the understanding of various interactions in electronic systems, such as the Seebeck coefficient, electrical conductivity, thermal conductivity and the power factor.

3.1. Electronic Properties

The electronic structure of any material is important in order to understand sub-atomic properties. This information is obtained from the calculated density of states (DOSs) and band structure via the materials' electron density. When carrying out calculations, energies were allowed to converge with respect to the k-points' density ($14 \times 14 \times 14$ for α -Cu₂S and $16 \times 16 \times 16$ for α -Cu₂Se) for the density of state, band structure and lattice calculations. In the process of structural optimization, all atoms were fully relaxed and the energy convergence threshold was 1.0×10^{-5} eV. The force convergence threshold of each atom was $0.015 \text{ eV} \cdot \text{Å}^{-1}$.

Figure 1a,b shows the total energy against the volume for the optimized structures of alpha-type copper sulphide (α -Cu₂S) (a) and copper selenide (α -Cu₂Se) (b), respectively. The calculated lattice constants, volume and energy are displayed in Table 1. The lattice constants of Cu₂S and Cu₂Se were found to be 10.39 and 10.89 Bohr (5.50 and 5.59 Å), corresponding to total energies of -3705.95 and -5735.90 eV, respectively. Bharathi et al. [18] calculated the lattice constant of Cu₂S and found it to be 5.60 Å, which differs from our results by 0.04%. Sakuma et al. [19] calculated the lattice constant of cubic Cu₂Se and found it to be 5.85 Å, which differs from our results by 0.36%.

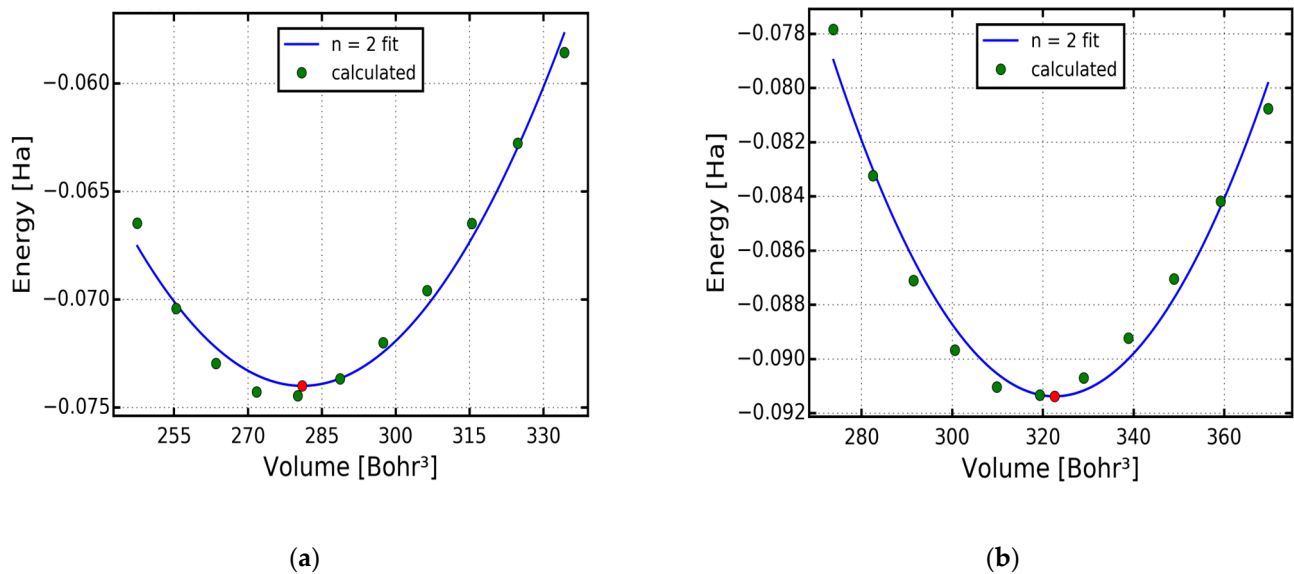


Figure 1. Change in total energy against volume. (a) Cubic copper sulphide (α -Cu₂S). (b) Cubic copper selenide (α -Cu₂Se). The red dots signify the actual minimum point values in both curves.

Table 1. Minimum volume (V) in Bohr³, lattice constant (a) in Bohr and minimum energy (E) in eV units.

	Cu ₂ S	Cu ₂ Se
V (Bohr ³)	281.02	322.57
a (Bohr)	10.39	10.89
E (eV)	−3705.95	−5735.90

Figure 2a,b presents the calculated electronic band structure of the cubic α -Cu₂S (a) and α -Cu₂Se (b) symmetries, respectively. As observed in the figures, there is an overlap at the bottom of the conduction and the top of the valence bands in the high symmetry k-points from L to Γ . As such, both α -Cu₂S and α -Cu₂Se compounds give rise to zero band gaps, which are associated with metallic behaviour, but this must be taken with caution as Tyagi et al. [8] and Råsander et al. [20] clarified that PBE_sol functional overestimation in the energy bands can be corrected by also considering hybrid functionals. The electronic density of state (DOS) results are displayed in Figure 3a,b. In both compounds, the valence band area has two notable regions: a lower energy region, which sweeps from −8.0 to −6.0 eV, and an upper energy region, which sweeps from −3.5 to 0.0 eV (Fermi level). In both α -Cu₂S and α -Cu₂Se, the electron charge density is distributed in the same way in the lower and upper regions. The lower region is associated with the core p and s states of Cu and S (or Se) in α -Cu₂S or (α -Cu₂Se). The upper region is associated with a mixture of d, p and valence s states. As observed in Figure 3a,b, the 3d peaks are outstanding between −3.0 and −2.0 eV in the upper region of the valence band. For α -Cu₂Se, the peaks are associated with a mixture of Cu and Se 3d states, whilst the peak on α -Cu₂S is associated with the lone Cu 3d states. The amalgamated results presented in Figure 3a,b are in agreement with the calculations of Råsander et al. [20] and the tight binding model computations of Garba and Jacobs [21].

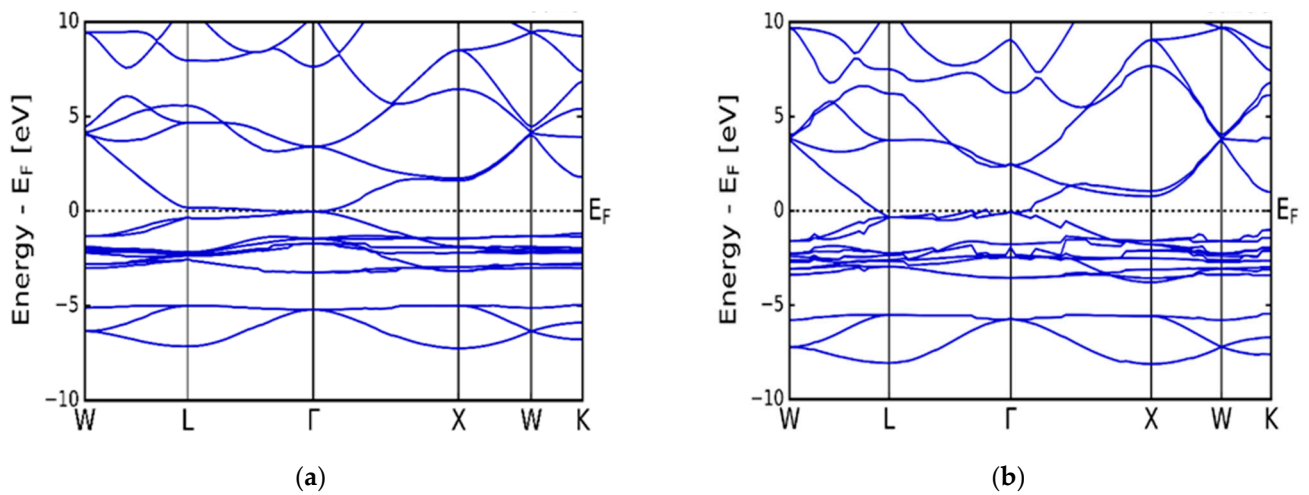


Figure 2. Calculated electronic band structures. (a) Cubic copper sulphide (α -Cu₂S). (b) Cubic copper selenide (α -Cu₂Se).

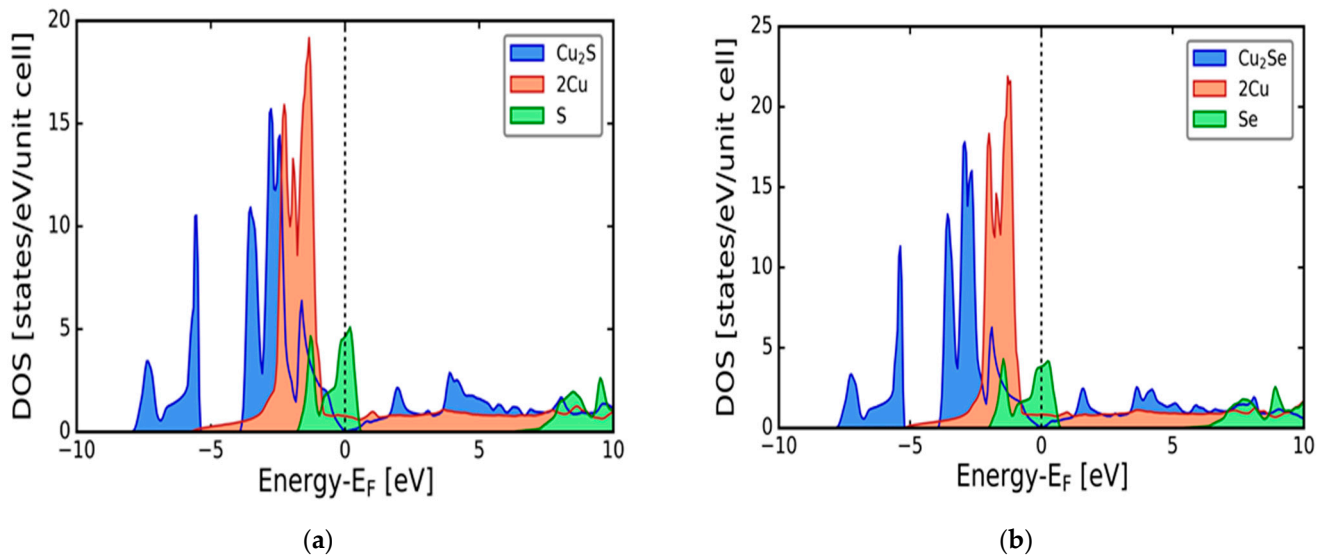


Figure 3. Calculated electronic density of states (DOS). (a) Cubic copper sulphide (α -Cu₂S). (b) Cubic copper selenide (α -Cu₂Se).

3.2. Elastic Properties

Systematically, the elastic properties of alpha Cu₂S and Cu₂Se were also computed. Such calculations assist in understanding the stability, stiffness, ductility and anisotropy of materials. Young’s modulus measures the stiffness of the materials, the bulk modulus refers to the resistance to shape deformation, the shear modulus reflects the resistance against the shear deformation and Poisson’s ratio predicts the ductility of the materials [22]. In cubic crystal symmetries, there are three independent elastic constants, which are C₁₁, C₁₂ and C₄₄. Theoretically, elastic constants can be calculated directly via the total ground-state energy $E_{TOT}(V, \epsilon)$ of the crystals, as discussed by Stadler et al. [23], or using the relation between stress (σ_{ij}) and strain (ϵ_{ij}) within a crystal, as proposed by Nielsen and Martin [24]. In this article, elastic constants are calculated using the ElaStic@exciting [13] interface, which can be used to obtain full elastic constants of any crystal system. In order to calculate the three elastic constants (C₁₁, C₁₂ and C₄₄), bulk modulus (B_0), Young’s modulus (Y), shear modulus (G) and Poisson’s ratio (ν), the following equation relations were considered [25]:

$$C_{11} + 2C_{12} = 3B_0 \quad (1)$$

In Equation (1), C_{11} is associated with the longitudinal compression, whereas C_{12} is associated with the transverse expansion.

$$G = C_{44} \tag{2}$$

In this Equation (2), C_{44} directly extracts the shear modulus (G) on adjacent planes.

$$Y = \frac{9B_0G}{3B_0 + G} \tag{3}$$

$$\nu = \frac{3B_0 - 2G}{2(3B_0 + G)} \tag{4}$$

In Equations (3) and (4), different operations on the bulk modulus (B_0) and shear modulus (G) produce the Young’s modulus and Poisson’s ratio, respectively.

Tables 2 and 3 present the calculated elastic constants of α -Cu₂S and α -Cu₂Se, respectively. In view of the fact that alpha Cu₂S and Cu₂Se are cubic materials, the elastic deformation’s stability needs to obey the following trend: $C_{11} > 0$; $C_{12} > 0$; $C_{11} - |C_{12}| > 0$ and $C_{44} > 0$ [3,25–27]. The values presented in Tables 2 and 3 confirm that all conditions of cubic deformation stability are satisfied. Making use of condition $C_{11} - |C_{12}| > 0$, a solid material can be predicted to obey either a homogeneous or anisotropic elastic property. If $C_{11} - C_{12} > 0$, the material complies with homogeneous elasticity, and if $C_{11} - C_{12} < 0$, the material conforms to anisotropic elasticity. Reflecting upon this condition, we can conclude that materials α -Cu₂S and α -Cu₂Se are mechanically stable and can also be viewed as belonging to homogeneous elastic media [26,27]. As portrayed in the tables, the bulk moduli of α -Cu₂S and α -Cu₂Se are much greater than the respective shear moduli, which leads to Poisson ratios of 0.35 and 0.44, respectively. Such positive values within the range of 0.0–0.5 suggest that both α -Cu₂S and α -Cu₂Se compounds can be stretched in one direction whilst they expand in two other directions that are perpendicular to the direction of compression [27]. Mott et al. [28] described that for incompressible materials, the bulk modulus (B_0) is typically large compared to the shear modulus (G), which results in a Poisson ratio of about 0.5. This notion suggests that both materials are incompressible, with α -Cu₂Se more incompressible than α -Cu₂S since the Poisson’s ratio of α -Cu₂Se is very close to 0.5 [28]. Aimed at α -Cu₂Se, the bulk, shear and Young’s modulus values are in agreement with the computational results [3] in comparison with the experimental results [26]. In the case of the α -Cu₂S compound, only computational results are available for comparison. Young’s modulus values suggest both α -Cu₂S and α -Cu₂Se materials as stiff [3]. Considering this entire discussion, all elastic constants conform to the expected mechanical stability relations in both compounds.

Table 2. Elastic constants (C_{11} , C_{12} and C_{44}), bulk modulus (B_0), Young’s modulus (Y) and shear modulus (G), all in GPa and Poisson’s ratio (ν) [26].

α -Cu ₂ S	C_{11}	C_{12}	C_{44}	B_0	Y	G	ν
This work (GPa)	105.940	54.680	23.442	71.767	63.421	23.442	0.3530
Computational (GPa)			-	80.70 ^a	65.413 ^a	23.692 ^a	0.360 ^a

^[a] Ref. [26].

Table 3. Elastic constants (C_{11} , C_{12} and C_{44}), bulk modulus (B_0), Young’s modulus (Y) and shear modulus (G), all in GPa and Poisson’s ratio (ν) [3,26,27].

α -Cu ₂ Se	C_{11}	C_{12}	C_{44}	B_0	Y	G	ν
This work (GPa)	120.11	110.49	16.540	113.70	47.320	16.540	0.4400
Computational (GPa)	121.298 ^b	73.419 ^b	74.101 ^b	89.276 ^b	53.57 ^c	20.58 ^b	0.300 ^b
Experimental (GPa)	72.80 ^c	-	-	45.70 ^c	34.20 ^c	13.60 ^c	0.390 ^c

^[b] Ref. [3]; ^[c] Ref. [26].

3.3. Transport Properties

The thermo-electric effect is a phenomenon that explains the ability of certain materials to transform solar energy into electrical energy. In order to understand the thermo-electric properties of α -Cu₂S and α -Cu₂Se materials at 300 K, a presentation of the Seebeck coefficient, electrical and thermal conductivities per relaxation time and the power factor is shown in Figure 4a–d. Figure 4a displays the behaviour of the Seebeck coefficient (S) against the chemical potential (μ), which indicates two notable maxima peaks for both materials. Symmetrically, the positive maximum S values of Cu₂S and Cu₂Se are $150 \mu\text{VK}^{-1}$ and $125 \mu\text{VK}^{-1}$, respectively, at $\mu = -0.05 \text{ eV}$, whilst the negative minima are $-100 \mu\text{VK}^{-1}$ and $-220 \mu\text{VK}^{-1}$, respectively, at $\mu = 0.05 \text{ eV}$. The calculated Seebeck coefficient provides good consistency with respect to the experimental outcomes of Byeon et al. [29], where the group studied Seebeck coefficients of Cu₂Se and discovered two negative peaks possessing a larger magnitude than the positive peak. Theoretically, on the chemical potential abscissa of Figure 4a, the positive and negative values suggest the electron (n-type) and hole (p-type) dopants, respectively [29]. Thus, for α -Cu₂S, p-type dopants are more elevated compared to n-type dopants, but for α -Cu₂Se, the n-type dopant overcomes p-type dopants. This proposes the concept that α -Cu₂S favours p-type conductivity, whilst α -Cu₂Se favours n-type conductivity. Intuitively, this suggests that p-type conductivity originates from the extra hole density from unoccupied S states in the upper region of the α -Cu₂S density of states. However, with respect to α -Cu₂Se, Se states present extra electron density, which coincides with the conduction band resulting in n-type conductivity.

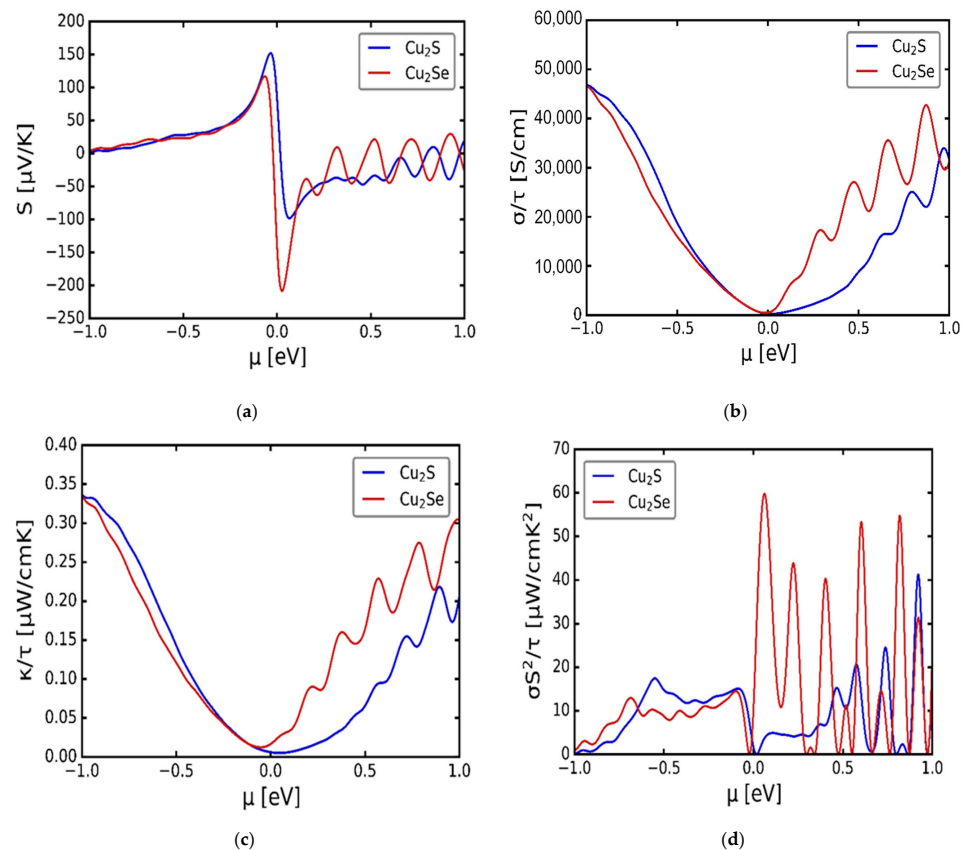


Figure 4. Thermo-electric transport properties of cubic α -Cu₂S and α -Cu₂Se, all at 300 K. (a) Variations in the Seebeck coefficient (S) against the chemical potential (μ). (b) Variations in electrical conductivity per relaxation time (σ/τ) against the chemical potential (μ). (c) Variations in thermal conductivity per relaxation time (κ/τ) against the chemical potential (μ). (d) Variations in the power factor per relaxation time ($\sigma S^2/\tau$) against the chemical potential (μ).

The electrical (σ/τ) and thermal (κ/τ) conductivities per relaxation time against the chemical potential (μ) appear in Figure 4b,c, respectively. Both curves display a similar behaviour relative to the changing μ , and their turning points occur at the Fermi level. Around the Fermi level, electrical conductivity suggests metallic behaviour as the curve does not entirely touch the zero level of the σ for both materials [30]. The power factor per relaxation time ($\sigma S^2/\tau$) quantity describes how efficient a given thermo-electric material is [30]. In Figure 4d, the observation of visible active peaks is evident in the positive zone of both α -Cu₂S and α -Cu₂Se compounds, even though the peaks for α -Cu₂S are somehow compromised. Such values suggest that the power factor is more inclined towards n-type conductivity for both α -Cu₂S and α -Cu₂Se. Mahan and Sofo's [16] findings expressed that a good thermo-electric material is expected to have a large Seebeck coefficient, high electrical conductivity and low thermal conductivity in order to acquire an enhanced figure of merit [16,30–32]. In this instance, for both α -Cu₂S and α -Cu₂Se, S exhibits high positive values of 150 μVK^{-1} and 125 μVK^{-1} , respectively, and the κ maximum values of 0.35 $\text{Wcm}^{-1}\text{K}^{-1}$ and 0.37 $\text{Wcm}^{-1}\text{K}^{-1}$, respectively, are sufficiently small. A conclusion is that the alpha Cu₂S and Cu₂Se satisfy the properties of being good thermo-electric materials.

Figure 5a,b shows variations in the Seebeck coefficient, with temperature at chemical potentials $\mu = -0.136$ and 0.136 eV, respectively, for α -Cu₂S and α -Cu₂Se. According to Scheidemantel et al. [31], the argument is that negative and positive chemical potentials are associated with p- and n-type conductivities, respectively. Considering Figure 5a, for cubic Cu₂S, p-type conductivity reflects the highest S value in relation to n-type conductivity. Furthermore, for p-type conductivity, S increases continuously with increasing temperatures up to about 155 μVK^{-1} at 1200 K. Conversely, for n-type conductivity, the S reaches a maximum of 100 μVK^{-1} around 600 K and then decreases towards about 75 μVK^{-1} at 1200 K. Narjis et al. [33] and, independently, Zhao et al. [34] pointed out that the positive values of the Seebeck coefficient indicate transport properties that are dominated by holes, suggesting p-type conductivity. On the other hand, the negative values of S indicate transport properties dominated by electrons, which suggest n-type conductivity materials. In this case, the suggestion that α -Cu₂S is a p-type conductivity material holds. Looking at Figure 5b, which represents α -Cu₂Se, n-type doping obtained higher negative S values than the p-type value. In addition, upon n-type doping, S values decrease exponentially with increasing temperatures, which suggests that α -Cu₂Se is an n-type material.

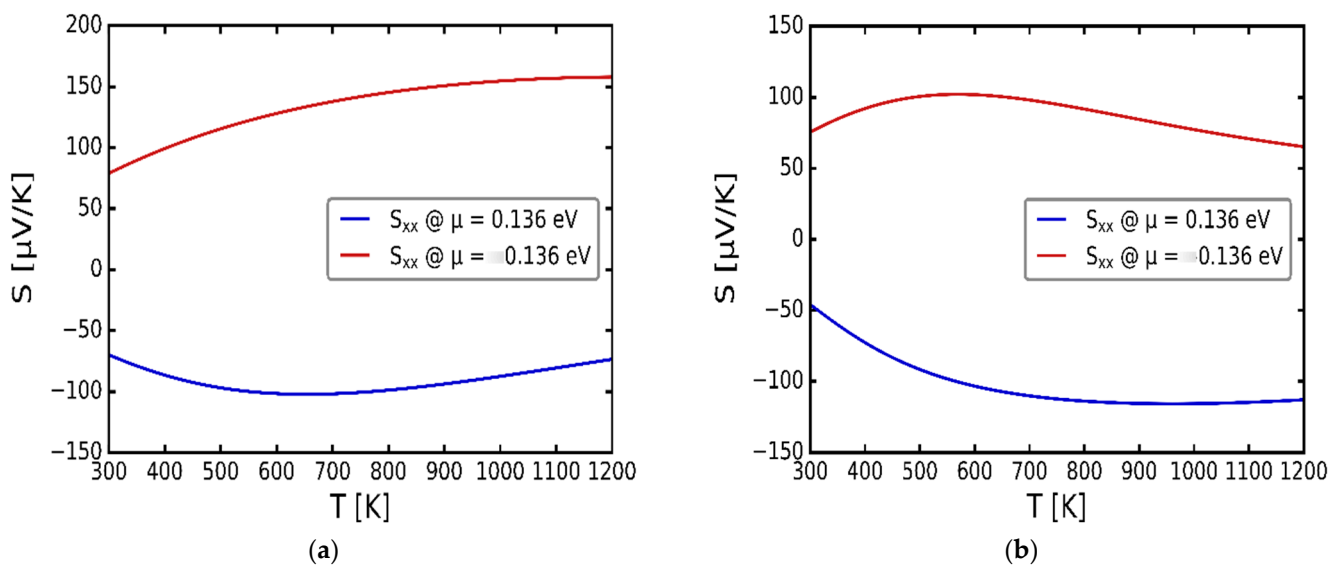


Figure 5. Variations in the Seebeck coefficient (S) with respect to temperature (T). (a) Cubic α -Cu₂S. (b) Cubic α -Cu₂Se.

As observed, Figure 6a,b displays electrical conductivities per relaxation time against the temperature at constant chemical potentials $\mu = -0.136$ and 0.136 eV of α -Cu₂S and α -Cu₂Se, respectively. Compatible with the Seebeck coefficient's performance, for α -Cu₂S, p-type doping at $\mu = -0.136$ eV demonstrates the highest electrical conductivity per relaxation time compared to n-type doping at $\mu = 0.136$ eV (Figure 6a). In a similar manner, in Figure 6b, for α -Cu₂Se, n-type doping displays the highest electrical conductivity per relaxation time compared to p-type doping. It must also be mentioned that in both instances of α -Cu₂S and α -Cu₂Se, the electrical conductivity per relaxation time at $\mu = -0.136$ and 0.136 eV increases with increasing temperature, which further suggests a metallic character [35].

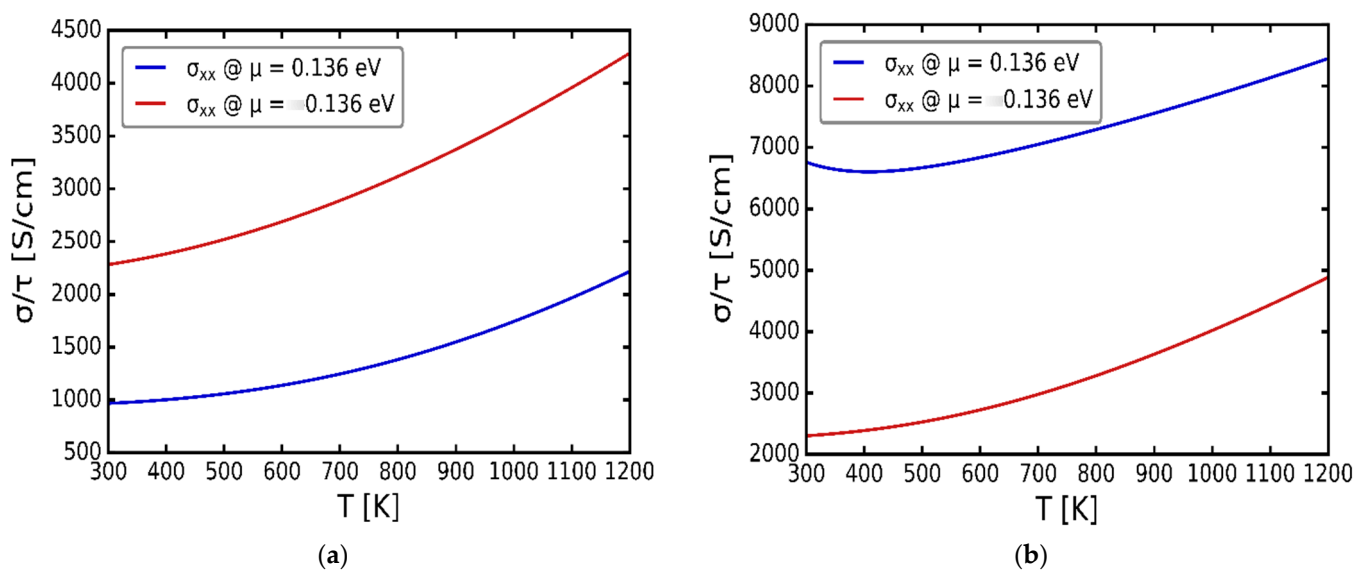


Figure 6. Variations in electrical conductivity per relaxation time (σ/τ) with temperature (T). (a) Cubic α -Cu₂S. (b) Cubic α -Cu₂Se.

Advancing onwards, Figure 7a,b presents thermal conductivities per relaxation time against temperature at chemical potentials $\mu = -0.136$ and 0.136 eV, respectively, for both α -Cu₂S and α -Cu₂Se. Previous studies by Jiang et al. [32] and Narjis et al. [33] clarified that a material with high electrical conductivity must have very low thermal conductivity. In accordance with this, Figure 7a shows that for α -Cu₂S, good thermal conductivity favours p-type doping since it exhibits the lowest thermal conductivity, whereas Figure 7b illustrates that the good thermal conductivity of α -Cu₂Se is obtained via n-type doping. At $\mu = -0.136$ and 0.136 eV, the thermal conductivity per relaxation time increases exponentially with increasing temperature for both α -Cu₂S and α -Cu₂Se. In addition, Figure 7a,b illustrates that the minimum thermal conductivities per relaxation time of alpha Cu₂S and Cu₂Se are still very low at values of about 0.02 and 0.05 Wcm⁻¹K⁻¹ at 300 K. Such a property further confirms that the thermal conductivity behaviour of α -Cu₂S is in line with some previous related studies [32–34].

Lastly, Figure 8a,b illustrates the power factor per relaxation time against temperature at chemical potentials $\mu = -0.136$ and 0.136 eV of α -Cu₂S and α -Cu₂Se, respectively. The power factor is the product of electrical conductivity and the square of the Seebeck coefficient. Hasan et al. [30] explained that if the maximum power factor was obtained at the hole-doping region ($\mu < 0$), then it could be concluded that the material works better as a p-type thermo-electric material. Similarly, when maximum power factor was obtained at the electron doping region ($\mu > 0$), the material worked well as an n-type thermo-electric material [30]. For α -Cu₂S in Figure 8a, p-type doping suggests a high power factor value compared to n-type doping. Moreover, n-type doping demonstrates a relatively constant power factor with increasing temperature, although the power factor

increases linearly as the temperature increases for p-type doping, which further confirms that α -Cu₂S indeed works better as a p-type thermo-electric material. In Figure 8b, which shows α -Cu₂Se curves, n-type doping suggests the highest power factor value related to p-type doping. Also, with respect to p-type doping, the power factor demonstrates the highest value at around 600 to 700 K and then lowers to 20 μ Wcm⁻¹K² at 1200 K, but for n-type doping, the power factor increases with increasing temperature. This also confirms that α -Cu₂Se works better as an n-type thermo-electric material. To summarize, all variations of transport coefficients with respect to temperature suggest α -Cu₂S as a good p-type conductive thermo-electric material, whilst α -Cu₂Se is a good n-type conductive thermo-electric material.

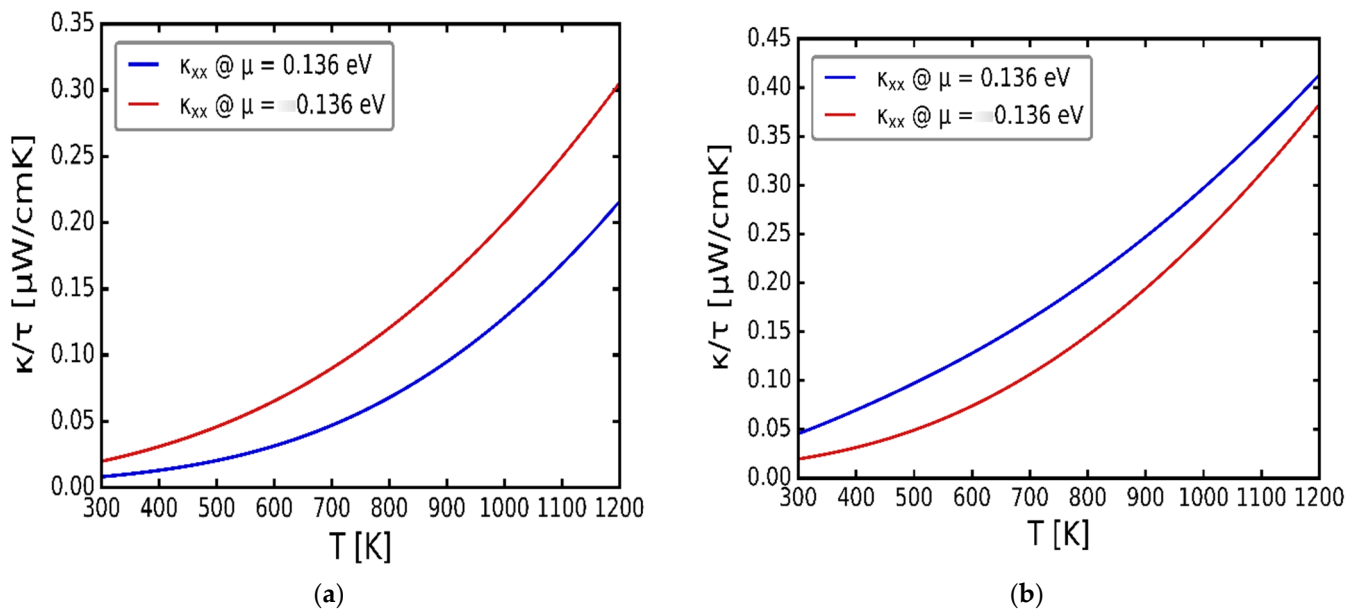


Figure 7. Variations in the thermal conductivity per relaxation time (κ/τ) with temperature (T). (a) Cubic α -Cu₂S. (b) Cubic α -Cu₂Se.

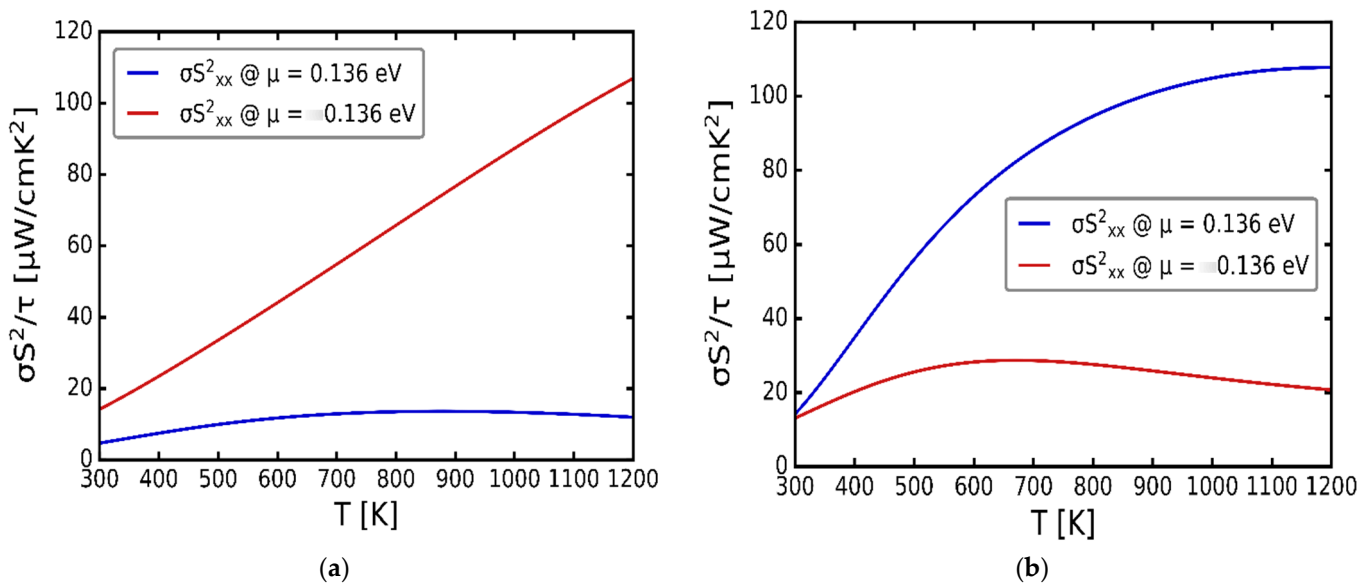


Figure 8. Variations in the power factor per relaxation time ($\sigma S^2/\tau$) with respect to temperature (T). (a) Cubic α -Cu₂S. (b) Cubic α -Cu₂Se.

4. Conclusions

The results of the electronic properties are in agreement with previous studies, showing alpha copper sulphide and copper selenide to possess metallic characters with zero-energy band gaps. This zero-energy band gap is attributed to the overlap of the lowest valence and the highest conduction bands' geometry between symmetry points L and Γ with respect to both materials. Apart from this, zero band gap compounds possess some exceptional and superior electronic properties associated with chemical sensing and information processing. Elastic constant results demonstrate these chalcogenides as mechanically stable, with low shear moduli coupled with high bulk moduli. Such material compositions are expected with respect to thermo-electric materials. However, care should be taken when choosing them as low shear and high bulk moduli often result in high thermal conductivity, which is not required in thermo-electric transport applications.

The transport properties of materials suggest p-type conductivity for α -Cu₂S and n-type conductivity for α -Cu₂Se. The high positive (α -Cu₂S) and negative (α -Cu₂Se) values of the Seebeck coefficient, high electrical conductivity, high thermal conductivity and low thermal conductivity with respect to the chemical potentials suggest that alpha Cu₂S and Cu₂Se are good thermo-electric transport materials for p-type and n-type doping, respectively. This is further corroborated by the low number of changes in electrical conductivity with respect to increasing temperatures. Very low and suppressed thermal conductivity values with respect to increasing temperatures further support these findings. Such low shear and high bulk moduli materials have potential in thermo-electric transport applications. To quantify these results, a combination of such n-type and p-type conductive materials suggest sustainable solar harvesting for prolonged electrical energy generation.

Author Contributions: Conceptualization, M.R. and T.M.; methodology, T.M.; formal analysis, M.R.; investigation, M.R.; resources, T.M.; data curation, M.R.; writing—original draft preparation, M.R.; writing—review and editing, T.M.; visualization, M.R.; supervision, T.M.; project administration, T.M.; funding acquisition, T.M. All authors have read and agreed to the published version of the manuscript.

Funding: This research was funded by the University of Limpopo.

Data Availability Statement: The data utilized in this article are available from the corresponding author upon request.

Acknowledgments: The University of Limpopo (UL) is thanked for the funding and the Centre for High Performance Computing (CHPC) for computational facilities.

Conflicts of Interest: The authors declare no conflict of interest.

References

1. Ashfaq, A.; Tahir, S.; ur Rehman, U.; Ali, A.; Ashfaq, H.F.; Ahmad, W.; Mushtaq, S.; Saeed, R.; Haneef, M.; Khan, K.M.; et al. Structural, morphological and thermoelectric properties of copper deficient and excessive Cu_{2-x}S nanoparticles with (x = 0–0.3). *Surf. Interfaces* **2022**, *30*, 101965. [[CrossRef](#)]
2. Dioum, A.; Diakite, Y.I.; Malozovsky, Y.; Ayirizia, B.A.; Beye, A.C.; Bagayoko, D. First-principles investigation of electronic and related properties of cubic magnesium silicide (Mg₂Si). *Computation* **2023**, *11*, 40. [[CrossRef](#)]
3. Namsani, S.; Gahtori, B.; Auluck, S.; Singh, J.K. An interaction potential to study the thermal structure evolution of a thermoelectric material: β -Cu₂Se. *J. Comput. Chem.* **2017**, *38*, 2161–2170. [[CrossRef](#)]
4. Potter, R.W. An electrochemical investigation of the system copper-sulfur. *Econ. Geol.* **1977**, *72*, 1524–1542. [[CrossRef](#)]
5. Will, G.; Hinze, E.; Abdelrahman, A.R.M. Crystal structure analysis and refinement of digenite, Cu_{1.8}S, in the temperature range 20 to 500 °C under controlled sulfur partial pressure. *Eur. J. Mineral.* **2002**, *14*, 591–598. [[CrossRef](#)]
6. Kim, H.; Ballikaya, S.; Chi, H.; Ahn, J.P.; Ahn, K.; Uher, C.; Kaviany, M. Ultralow thermal conductivity of β -Cu₂Se by atomic fluidity and structure distortion. *Acta Mater.* **2015**, *86*, 247–253. [[CrossRef](#)]
7. Tyagi, K.; Gahtori, B.; Bathula, S.; Auluck, S.; Dhar, A. Band structure and transport studies of copper selenide: An efficient thermoelectric material. *Appl. Phys. Lett.* **2014**, *105*, 173905. [[CrossRef](#)]
8. Nelson, H.D.; Li, X.; Gamelin, D.R. Computational studies of the electronic structures of copper-doped CdSe nanocrystals: Oxidation states, Jahn-Teller distortions, Vibronic bandshapes, and Singlet-triplet splittings. *J. Phys. Chem. C* **2016**, *120*, 5714–5723. [[CrossRef](#)]

9. He, Y.; Day, T.; Zhang, T.; Liu, H.; Shi, X.; Chen, L.; Snyder, G.J. High thermoelectric performance in non-toxic earth-abundant copper sulfide. *Adv. Mater.* **2014**, *26*, 3974–3978. [[CrossRef](#)]
10. Arora, S.; Kabra, K.; Joshi, K.B.; Sharma, B.K.; Sharma, G. Structural, elastic, thermodynamic and electronic properties of covellite, CuS. *Phys. B Condens. Matter* **2020**, *582*, 311142. [[CrossRef](#)]
11. Lv, Z.; Cui, H.; Huang, H.; Li, X.; Wang, H.; Ji, G. Study of the electronic, bonding, elastic and acoustic properties of covellite via first principles. *J. Alloys Compd.* **2017**, *692*, 440–447. [[CrossRef](#)]
12. Tang, Y.Q.; Ge, Z.H.; Feng, J. Synthesis and thermoelectric properties of copper sulfides via solution phase methods and spark plasma sintering. *Crystals* **2017**, *7*, 141. [[CrossRef](#)]
13. Gulans, A.; Kontur, S.; Meisenbichler, C.; Nabok, D.; Pavone, P.; Rigamonti, S.; Sagmeister, S.; Werner, U.; Draxl, C. Exciting: A full-potential all-electron package implementing density-functional theory and many-body perturbation theory. *J. Phys. Condens. Matter* **2014**, *26*, 363202. [[CrossRef](#)] [[PubMed](#)]
14. Perdew, J.P.; Chevary, J.A.; Vosko, S.H.; Jackson, K.A.; Pederson, M.R.; Singh, D.J.; Fiolhais, C. Atoms, molecules, solids, and surfaces: Applications of the generalized gradient approximation for exchange and correlation. *Phys. Rev. B* **1992**, *46*, 6671–6687. [[CrossRef](#)]
15. Perdew, J.P.; Ruzsinszky, A.; Csonka, G.I.; Vydrov, O.A.; Scuseria, G.E.; Constantin, L.A.; Zhou, X.; Burke, K. Restoring the density-gradient expansion for exchange in solids and surfaces. *arXiv* **2007**, arXiv:0707.2088v2. [[CrossRef](#)]
16. Mahan, G.D.; Sofo, J.O. The best thermoelectric. *Proc. Natl. Acad. Sci. USA* **1996**, *93*, 7436–7439. [[CrossRef](#)]
17. Aroyo, M.L.; Perez-Mato, J.M.; Capillas, C.; Kroumova, E.; Ivantchev, S.; Madariaga, G.; Kirov, A.; Wondratschek, H. Bilbao crystallographic server I: Databases and crystallographic computing programs. *Z. Krist.* **2006**, *221*, 15–27.
18. Bharathi, B.; Thanikaikarasan, S.; Ramesh, K. Structural, compositional, and optical properties of electrochemically deposited Cu₂S thin films. *Int. J. ChemTech Res.* **2014**, *6*, 1907–1909.
19. Sakuma, T.; Sugiyama, K.; Matsubara, E.; Waseda, Y. Determination of the Crystal Structure of Superionic Phase of Cu₂Se. *Mater. Trans. JIM* **1989**, *30*, 365–369. [[CrossRef](#)]
20. Räsander, M.; Bergqvist, L.; Delin, A. Density functional theory study of the electronic structure of fluorite Cu₂Se. *J. Phys. Condens. Matter* **2013**, *25*, 125503. [[CrossRef](#)]
21. Garba, E.J.D.; Jacobs, R.L. The electronic structure of Cu_{2-x}Se. *Phys. B+C* **1986**, *138*, 253–260. [[CrossRef](#)]
22. Zeng, X.; Peng, R.; Yu, Y.; Hu, Z.; Wen, Y.; Song, L. Pressure effect on elastic constants and related properties of Ti₃Al intermetallic compound: A first-principles study. *Materials* **2018**, *11*, 2015. [[CrossRef](#)] [[PubMed](#)]
23. Stadler, R.; Wolf, W.; Podloucky, R.; Kresse, G.; Furthmüller, J.; Hafner, J. Ab initio calculations of cohesive, elastic, and dynamical properties of CoSi₂ by pseudopotential and all-electrons techniques. *Phys. Rev. B* **1996**, *54*, 1729–1734. [[CrossRef](#)] [[PubMed](#)]
24. Nielsen, O.H.; Martin, R.M. First-principles calculation of stress. *Phys. Rev. Lett.* **1983**, *50*, 697–700. [[CrossRef](#)]
25. Jamal, M.; Asadabadi, S.J.; Ahmad, I.; Aliabad, H.R. Elastic constants of cubic crystals. *Comput. Mater. Sci.* **2014**, *95*, 592–599. [[CrossRef](#)]
26. Hasan, S.; Baral, K.; Ching, W.Y. Total bond order density as a quantum mechanical metric for materials design: Application to chalcogenide crystals. *Preprints* **2019**, 2019060199. [[CrossRef](#)]
27. Zhang, J.; Zhang, C.; Zhu, T.; Yan, Y.; Su, X.; Tang, X. Mechanical properties and thermal stability of the high-thermoelectric-performance Cu₂Se compound. *ACS Appl. Mater. Interfaces* **2021**, *13*, 45736–45743. [[CrossRef](#)]
28. Mott, P.H.; Dorgan, J.R.; Roland, C.M. The bulk modulus and Poisson’s ratio of “incompressible” materials. *J. Sound Vib.* **2008**, *312*, 572–575. [[CrossRef](#)]
29. Byeon, D.; Sobota, R.; Delime-Codrin, K.; Choi, S.; Hirata, K.; Adachi, M.; Kiyama, M.; Matsuura, T.; Yamamoto, Y.; Matsunami, M.; et al. Discovery of colossal Seebeck effect in metallic Cu₂Se. *Nat. Commun.* **2019**, *10*, 72. [[CrossRef](#)]
30. Hasan, S.; San, S.; Baral, K.; Li, N.; Rulis, P.; Ching, W.Y. First-Principles Calculations of Thermoelectric Transport Properties of Quaternary and Ternary Bulk Chalcogenide Crystals. *Materials* **2022**, *15*, 2843. [[CrossRef](#)]
31. Scheidemann, T.J.; Ambrosch-Draxl, C.; Thonhauser, T.; Badding, J.V.; Sofo, J.O. Transport coefficients from first-principles calculations. *Phys. Rev. B* **2003**, *68*, 125210. [[CrossRef](#)]
32. Jiang, Q.; Yan, H.; Khaliq, J.; Shen, Y.; Simpson, K.; Reece, M.J. Enhancement of thermoelectric properties by atomic-scale percolation in digenite Cu_xS. *J. Mater. Chem. A* **2014**, *2*, 9486–9489. [[CrossRef](#)]
33. Narjis, A.; Outzourhit, A.; Aberkouks, A.; El Hasnaoui, M.; Nkhaili, L. Structural and thermoelectric properties of copper sulphide powders. *J. Semicond.* **2018**, *39*, 122001. [[CrossRef](#)]
34. Zhao, L.D.; Berardan, D.; Pei, Y.L.; Byl, C.; Pinsard-Gaudart, L.; Dragoe, N. Bi_{1-x}Sr_xCuSeO oxyselenides as promising thermoelectric materials. *Appl. Phys. Lett.* **2010**, *97*, 092118. [[CrossRef](#)]
35. Yang, D.; Su, X.; Yan, Y.; He, J.; Uher, C.; Tang, X. Mechanochemical synthesis of high thermoelectric performance bulk Cu₂X (X = S, Se) materials. *APL Mater.* **2016**, *4*, 116110. [[CrossRef](#)]

Disclaimer/Publisher’s Note: The statements, opinions and data contained in all publications are solely those of the individual author(s) and contributor(s) and not of MDPI and/or the editor(s). MDPI and/or the editor(s) disclaim responsibility for any injury to people or property resulting from any ideas, methods, instructions or products referred to in the content.